

Stellar neutron capture cross sections of ^{41}K and ^{45}Sc

M. Heil,^{1,*} R. Plag,¹ E. Uberseder,² S. Bisterzo,^{3,4} F. Käppeler,⁵ A. Mengoni,⁶ and M. Pignatari^{7,8,†}

¹*GSI Helmholtzzentrum für Schwerionenforschung GmbH, Darmstadt, Germany*

²*University of Notre Dame, Notre Dame, Indiana, USA*

³*INAF, Astrophysical Observatory of Turin, 10025 Pino Torinese, Italy*

⁴*INFN, Sezione di Torino, Via P. Giuria 1, 10125 Torino, Italy*

⁵*Karlsruhe Institute of Technology (KIT), Campus North, Institute of Nuclear Physics, P.O. Box 3640, Karlsruhe, Germany*

⁶*CERN, CH-1211 Geneva 23, Switzerland*

⁷*E. A. Milne Centre for Astrophysics, Department of Physics & Mathematics, University of Hull, Hull HU6 7RX, United Kingdom*

⁸*Konkoly Observatory, Research Centre for Astronomy and Earth Sciences, Hungarian Academy of Sciences, H-1121 Budapest, Hungary*

(Received 11 January 2016; published 24 May 2016)

The neutron capture cross sections of light nuclei ($A < 56$) are important for s -process scenarios since they act as neutron poisons. We report on measurements of the neutron capture cross sections of ^{41}K and ^{45}Sc , which were performed at the Karlsruhe 3.7 MV Van de Graaff accelerator via the activation method in a quasistellar neutron spectrum corresponding to a thermal energy of $kT = 25$ keV. Systematic effects were controlled by repeated irradiations, resulting in overall uncertainties of less than 3%. The measured spectrum-averaged data have been used to normalize the energy-dependent (n, γ) cross sections from the main data libraries JEFF-3.2, JENDL-4.0, and ENDF/B-VII.1, and a set of Maxwellian averaged cross sections was calculated for improving the s -process nucleosynthesis yields in AGB stars and in massive stars. At $kT = 30$ keV, the new Maxwellian averaged cross sections of ^{41}K and ^{45}Sc are 19.2 ± 0.6 mb and 61.3 ± 1.8 mb, respectively. Both values are 20% lower than previously recommended. The effect of neutron poisons is discussed for nuclei with $A < 56$ in general and for the investigated isotopes in particular.

DOI: [10.1103/PhysRevC.93.055807](https://doi.org/10.1103/PhysRevC.93.055807)

I. INTRODUCTION

The light elements between ^{12}C and ^{56}Fe are important for the s -process scenario because they affect the neutron balance inside stars. Although their neutron capture cross sections are small, these elements are much more abundant than those in the mass region above Fe. Therefore, light elements constitute potential neutron poisons and may consume neutrons, which are then not available for s -process nucleosynthesis. Especially important in this respect are neutron captures on the CNO elements and on the neon and magnesium isotopes, but also other light isotopes up to iron contribute as well.

The poisoning effect of the light isotopes between ^{12}C and ^{56}Fe can be illustrated at the example of thermally pulsing low-mass asymptotic giant branch (AGB) stars, where the s process takes place in two situations: between thermal instabilities via the $^{13}\text{C}(\alpha, n)^{16}\text{O}$ reaction in the so-called ^{13}C pocket at rather mild temperatures of about 90 MK and at the maximum extent of the thermal pulses via the $^{22}\text{Ne}(\alpha, n)^{25}\text{Mg}$ reaction at temperatures near 250 MK [1,2]. The first episode contributes about 95% to the overall neutron balance at comparably low neutron densities of 10^6 to 10^8 cm^{-3} . The second episode

starts with neutron densities of about 10^{11} cm^{-3} , which rapidly decrease during the thermal instability. This second episode is important for shaping the final s -process abundance pattern [3].

In AGB stars of 1.5 to 3 solar masses ($M = 1.5\text{--}3M_{\odot}$), which produce the main component of the s -process abundance distribution [4], the light isotopes consume around 35% of the available neutrons during the ^{13}C -pocket phase and about 65% during thermal instabilities. This poisoning effect is even higher in stars of lower metallicity, i.e., stars formed earlier during galactic evolution. In models with neutron/seed ratios about 10 times lower than solar, the corresponding fractions reach about 75% and 90% during the above episodes, respectively.

Neutron capture cross sections of light isotopes also play an important role in analyses of presolar grains, which can provide stringent constraints for s -process models [5,6]. Because these grains are only a few μm in size and because the abundances of heavy elements are rather low, their isotopic abundance components in the grains are difficult to analyze. Lighter elements are more abundant and, therefore, easier to detect. Among other elements lighter than Fe, isotopic abundances in presolar grains are reported for K, Ca, and Ti, in the mass region of ^{41}K and ^{45}Sc .

For many of these isotopes the neutron capture cross sections are not known with sufficient accuracy for a thorough discussion of these aspects of the s process and other neutron capture processes. In most cases, these cross sections are small and difficult to measure, and often dominated by strong resonances. Also direct radiative capture (DRC) components, which are not accessible by neutron time-of-flight (TOF) experiments, can contribute significantly.

*Corresponding author: m.heil@gsi.de

†Also with the NuGrid Collaboration, <http://www.nugridstars.org>

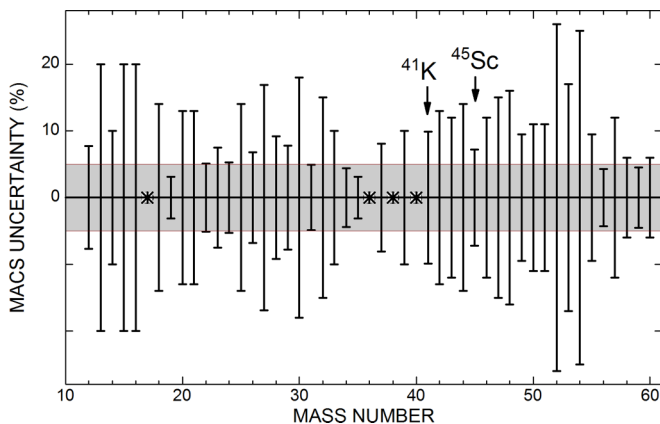


FIG. 1. Uncertainties of Maxwellian averaged cross sections for $kT = 30$ keV in the mass range between ^{12}C and ^{60}Ni [7]. The grey shaded bar indicates the $\pm 5\%$ uncertainty band that is commonly considered necessary for reliable predictions of the s abundance distribution. Experimental data are still missing for ^{17}O , ^{36}Cl , ^{38}Ar , and ^{40}K (stars).

Figure 1 shows the uncertainties of Maxwellian averaged capture cross sections (MACS) in the mass region from ^{12}C to ^{60}Ni as quoted in the KADoNiS compilation [7] for a thermal energy of $kT = 30$ keV.

In contrast to many accurate measurements for heavy nuclei, especially in the rare-earth region, practically all light nuclei exhibit rather large cross section uncertainties, and in some cases experimental data are even missing. For the quantitative assessment of their role as neutron poisons, accurate (n, γ) cross sections for the light elements are mandatory. Therefore, a series of measurements was performed at the Karlsruhe Van de Graaff accelerator in the mass range $12 \leq A \leq 60$. Results of this program have been published for ^{14}C , [8], ^{19}F [9], and $^{20,21,22}\text{Ne}$ [10] as well as preliminary data for ^{41}K and ^{45}Sc [11].

In this paper we present the final (n, γ) cross sections of ^{41}K and ^{45}Sc performed at the Karlsruhe 3.7 MV Van de Graaff accelerator. The measurements are described in Sec. III, and the results are compared in Sec. IV with previous data and current evaluations. The MACS values derived from these results are presented in Sec. V. In Sec. VI, the impact of neutron captures by the light nuclei from ^{12}C to ^{60}Ni is investigated to identify the crucial neutron poisons for the s process in general and for ^{41}K and ^{45}Sc in particular. A brief summary and outlook are given in Sec. VII.

II. PREVIOUS DATA

^{41}K : All but one of the five experimental data sets for the (n, γ) cross section of ^{41}K in the astrophysically relevant energy range between about 1 and 300 keV were determined via the activation method some 40 years ago. The work of Stuepegia *et al.* [12] was devoted to neutron energies above 162 keV, therefore overlapping only marginally with the region of interest here, whereas earlier measurements [13–15] were centered at neutron energies around 25 keV. Conditioned by the experimental possibilities at the time, rather large uncertainties

of 17% [15] and 23% [14] had to be admitted or only an upper limit could be given [13].

Consequently, the energy dependence of the cross section listed in the evaluated data libraries, e.g., JEFF-3.2 [16] and JENDL-4.0 [17], is based on the only TOF measurement by Macklin in the energy range from 11 eV to 2 MeV [18], which claimed systematic uncertainties of only 3% to 4%. Nevertheless, the evaluated cross sections differ by more than a factor of 2 (see Sec. V).

^{45}Sc : Activation measurements have been reported at 25 keV [14] and in the neutron energy range between 140 keV and 14 MeV [19]. Similarly to the situation for ^{41}K , these early measurements suffer from significant uncertainties of $\geq 50\%$ in the first and $\sim 25\%$ in the second case. TOF results have been obtained with a lead slowing-down spectrometer between 0.1 and 42 keV [20] (no uncertainties given) and at the Oak Ridge electron linac between 2.5 and 100 keV with uncertainties of about 10% [21]. The cross section data of these measurements exhibit a similar energy dependence, but differ in magnitude by about 30%. Because of the lower uncertainties and the much better neutron energy resolution, the Oak Ridge data have been considered for the current evaluations in the JEFF-3.2 [16], ENDF/B-VII.1 [22], and JENDL-4.0 [17] libraries.

In view of the problems with previous data, this work aims at measuring spectrum-averaged cross sections with considerably improved accuracy for direct use in astrophysical applications as well as for renormalization of previous TOF data.

III. ACTIVATION MEASUREMENTS

The activation method provides a reliable and accurate approach for measuring Maxwellian averaged cross sections at $kT = 25$ keV. Using the $^7\text{Li}(p, n)^7\text{Be}$ reaction for neutron production, a quasistellar spectrum can be produced that closely resembles a thermal spectrum with $kT = 25$ keV [23,24]. For a proton beam energy of $E_p = 1912$ keV, all neutrons are emitted in the direction of the proton beam, covering a cone with an opening angle of 120° . The neutron production target consists of a metallic Li layer $30 \mu\text{m}$ in thickness, which is evaporated onto a water-cooled copper backing. With proton beam intensities of typically $100 \mu\text{A}$ from the Karlsruhe 3.7 MV Van de Graaff accelerator, the neutron yield was $(2\text{--}3) \times 10^9 \text{ s}^{-1}$.

The Sc samples were prepared from high-purity metal foils $30 \mu\text{m}$ in thickness. As KBr was only available as a fine powder, this material was pressed into pellets about 0.25 and 0.5 mm in thickness. Different sample dimensions (Table I) were chosen to control systematic uncertainties due to the irradiation geometry and to self-absorption effects. For defining the neutron flux, each sample was sandwiched between $30\text{-}\mu\text{m}$ -thick gold monitor foils of the same diameter.

During the irradiations the samples were placed inside the neutron cone as sketched in Fig. 2. Throughout the irradiation, the relative neutron flux was recorded by a ^6Li glass detector at a distance of 83 cm from the target. With these data, beam-related fluctuations of the neutron flux could be properly considered for the decay correction of the induced activity during the irradiations.

TABLE I. Sample characteristics and irradiation parameters.

Activation	Composition	Mass (mg)	Diameter (mm)	Irradiation time (min)	Neutron fluence (10^{14})
1	Sc metal	2.43	6	2829	5.019
2	Sc metal	6.37	10	4148	3.352
3	Sc metal	9.57	12	2829	1.855
4	KBr	98.70	6	156	0.2681
5	KBr	733.27	12	1118	0.7069

After irradiation the induced sample activity was counted in a separate laboratory with a well-shielded high-purity germanium (HPGe) detector of 30% relative efficiency. Summing effects have been avoided by the comparably large distance of 76 mm between sample and detector. The γ efficiency was calibrated with a set of standard sources. In the relevant γ -energy range between 400 and 1200 keV, the efficiency was determined with an uncertainty of 2%.

The total number of activated nuclei A is determined by

$$A = \Phi N \sigma f_b \quad (1)$$

where $\Phi = \int \phi(t) dt$ is the neutron fluence applied in the irradiation, N the number of sample atoms per cm^2 , and σ the spectrum averaged neutron capture cross section.

The neutron fluence was determined via the well-established (n, γ) cross section of ^{197}Au , which was adopted from KADoNiS v1.0 [25]. Between $kT = 5$ and 50 keV it was derived by the weighted average of recent measurements at GELINA [26] and n_TOF [27,28] and in the range $kT = 60$ –100 keV by the average of the evaluated cross sections from the data libraries JEFF-3.2, JENDL-4.0, and ENDF/B-VII.1. This choice is in perfect agreement with a new activation measurement by the group in Sevilla [29]. Folding of the energy-differential gold cross section with the quasistellar neutron spectrum used in this work yields an effective value of 632 ± 9 mb, and reflects a 5.3% increase compared to the reference used in activation experiments prior to 2014.

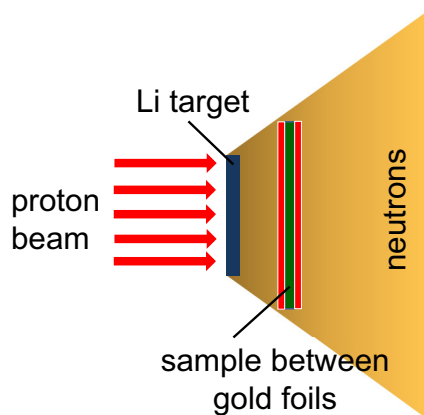


FIG. 2. Sketch of the experimental setup used in the neutron irradiations.

In Eq. (1) the factor

$$f_b = \frac{\int_0^{t_a} \Phi(t) e^{-\lambda(t_a-t)} dt}{\int_0^{t_a} \Phi(t) dt}$$

accounts for fluctuations of the neutron flux and for the decay during activation [23].

The total number of activated nuclei, A_γ , was calculated from the number of counts in the characteristic γ -ray lines listed in Table II,

$$C_\gamma = AK_\gamma \varepsilon_\gamma I_\gamma [1 - \exp(-\lambda t_m)] \exp(-\lambda t_w), \quad (2)$$

where ε_γ is the efficiency of the Ge detector, I_γ the intensity of the γ line, t_w the waiting time between irradiation and counting, and t_m the duration of the activity measurement.

The factor K_γ describes the γ -ray self-absorption in the sample. For disk samples and a small solid angle between sample and detector [33],

$$K_\gamma = \frac{1 - e^{-\mu x}}{\mu x}, \quad (3)$$

where μ is the γ -ray self absorption coefficient (adopted from Ref. [34]) and x the sample thickness. For the thin samples used in this work, the absorption losses were negligible for Sc and Au and well below 2% for the thicker KBr sample.

The systematic uncertainties of the activations are summarized in Table III. For both reactions the fluence determination represents the dominant systematic uncertainty. The statistical uncertainties were of the order of 1% in the Sc runs and 2% to 5% in the K activations (Table IV).

IV. RESULTS AND DISCUSSION

The measured spectrum-averaged cross sections (SACS) derived from the Sc and K activations are summarized in Table IV.

For both reactions the individual results, which were obtained with samples of different dimensions and with different

TABLE II. Decay properties of the product nuclei.

Product nucleus	Half-life (min)	E_γ (keV)	I_γ (%)	Reference
^{42}K	741.6 ± 0.72	1524.6	18.08 ± 0.09	[30]
^{46}Sc	120658 ± 58	889.28	99.984 ± 0.001	[31]
		1120.55	99.987 ± 0.001	
^{198}Au	3881.1 ± 0.3	411.8	95.58 ± 0.12	[32]

TABLE III. Compilation of systematic uncertainties.

Source of Uncertainty	Uncertainty (%)		
	Au	⁴¹ K	⁴⁵ Sc
Gold cross section	1.4		
Number of nuclei	0.6	0.1	0.4
Time factors, $f_w, f_m, f_b, \tau_{1/2}$	<0.1	<0.1	<0.1
Self-absorption	<0.1	<0.1	<0.1
Detector efficiency	1.5	1.5	1.5
Intensity per decay, I_γ	0.13	0.5	<0.01
Neutron fluence		2.2	2.2
Total systematic uncertainty		2.7	2.7

neutron fluences, are consistent within the quoted uncertainties thus validating the data analysis procedures. The statistical uncertainties were small enough that the overall uncertainties are dominated by systematic effects. In total, accuracies better than 3% and 4% could be obtained for the SACS values of ⁴⁵Sc and ⁴¹K, respectively. As shown by the comparison in Table V, the present results represent a significant improvement compared to previous activations [14,15,20]. This is illustrated for ⁴⁵Sc in Fig. 3, where the present uncertainty corresponds to the size of the symbol.

High-resolution TOF measurements have been reported for ⁴⁵Sc [21] and ⁴¹K [18] with uncertainties of about 10% and 3.3%, respectively. Although compatible within uncertainties, it is interesting to note that the results of both experiments are systematically larger than the present values. A possible explanation could be the sensitivity of older TOF experiments to sample-scattered neutrons, which are captured in the detector and/or in surrounding materials. This problem could give rise to significant background problems, especially for light nuclei, where the scattering/capture ratios are large [35–37].

V. MAXWELLIAN AVERAGED CROSS SECTIONS

The effective cross section in a stellar plasma is defined by the average over the Maxwell-Boltzmann distribution as

$$\langle \sigma \rangle_{kT} = \frac{\langle \sigma v \rangle}{v_T} = \frac{2}{\sqrt{\pi}} \frac{\int_0^\infty \sigma(E_n) E_n \exp(-E_n/kT) dE_n}{\int_0^\infty E_n \exp(-E_n/kT) dE_n} \quad (4)$$

TABLE IV. Measured cross sections and related statistical and systematic uncertainties.

Activation	E_γ (keV)	K_γ	Cross section (mb)	Mean value (mb)
⁴⁵ Sc(n,γ) ⁴⁶ Sc				
1	889.28	1.00	64.0 ± 0.9 ± 1.8	
	1120.55	1.00	66.5 ± 1.0 ± 1.9	
2	889.28		64.4 ± 0.7 ± 1.8	
	1120.55		65.8 ± 0.7 ± 1.8	
3	889.28		65.0 ± 0.7 ± 1.8	
	1120.55		64.7 ± 0.8 ± 1.8	65.0 ± 1.8
⁴¹ K(n,γ) ⁴² K				
4	1524.6	0.99	22.0 ± 1.6 ± 0.7	
5	1524.6	0.98	21.8 ± 0.5 ± 0.6	21.9 ± 0.8

TABLE V. Comparison of the present results with previous (n,γ) cross sections. “M-B” denotes Maxwell-Boltzmann.

E_n (keV)	σ_{exp} (mb)	Reference
⁴⁵ Sc(n,γ) ⁴⁶ Sc		
24 ± 5	56 ± 3	[14]
25 ± 5	50 ^a	[20]
25 ± 5	76 ± 8	[21]
25 (quasi M-B)	65.0 ± 1.8	This work
⁴¹ K(n,γ) ⁴² K		
24 ± 5	22 ± 5	[14]
24 ^b	30 ± 5	[15]
$kT = 25^c$	24.1 ± 0.8	[18]
25 (quasi M-B)	21.9 ± 0.8	This work

^aUncertainty not given.

^bSb-Be source, spectral range not given.

^cExtrapolated from $kT = 30$ keV value in reference.

where E_n denotes the neutron energy in the center-of-mass system, $\sigma(E_n)$ the energy-dependent neutron capture cross section, and kT the thermal energy.

The measured SACS values are a good approximation of the true stellar average only for thermal energies near $kT = 25$ keV, where the quasistellar neutron spectrum resembles closely the perfect thermal case. To obtain the MACS values for all relevant s -process temperatures, i.e., for the range of thermal energies between 5 and 100 keV, the present results have been used to normalize the evaluated cross sections.

For ⁴¹K the latest evaluations are those from the JEFF-3.2 [16] and JENDL-4.2 [17] cross section libraries. Surprisingly, the mean values of the evaluated cross sections over the experimental spectrum differ by more than a factor of 2, as indicated in Table VI. Nevertheless, the energy dependence of the cross sections is almost identical because both evaluations are using the TOF results of [18]. Accordingly, normalization with factors of 1.54 and 0.61 (Table VI) yields identical MACS data independent of kT . The adopted values are given in Table VII.

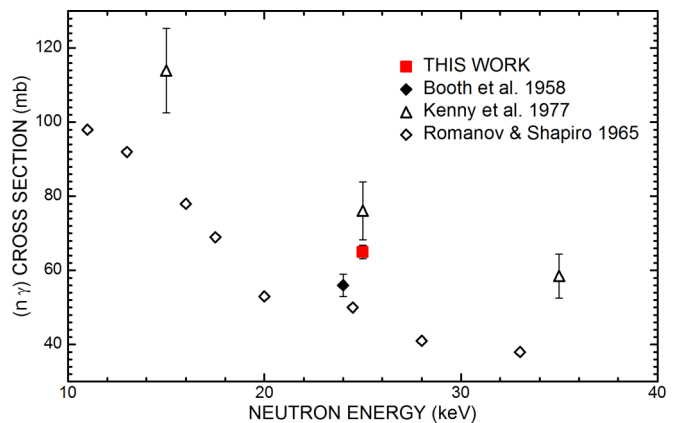


FIG. 3. Comparison of the measured ⁴⁵Sc cross section with a previous activation (Booth *et al.* [14]) and with TOF data by Romanov and Shapiro [20] (original resolution) and Kenny *et al.* [21] (averaged over 10 keV bins).

TABLE VI. Spectrum-averaged cross sections (in mb) and normalization factors NF for evaluated data.

	$^{41}\text{K}(n,\gamma)^{42}\text{K}$	NF	$^{45}\text{Sc}(n,\gamma)^{46}\text{Sc}$	NF
This work	21.9 ± 0.8		65.0 ± 1.8	
JEFF-3.2	14.2	1.54	68.3	0.95
JENDL-4.0	35.7	0.61	68.3	0.95

For ^{45}Sc , the situation is more complicated. Although equal SACS values for the experimental spectrum have been calculated from the evaluated cross sections (Table VI), the respective MACS results exhibit a slightly different trend with thermal energy as shown in Table VIII. As the reason for the differences is unclear and because the data are similar, the three data sets are simply averaged for the adopted final results in Table VIII.

For the MACS uncertainties the effect of the extrapolation to lower and higher thermal energies has to be added to the 3% systematic uncertainty of the present cross section measurement. As the energy dependence of both cross sections is determined by high-resolution TOF measurements [18,21], the extrapolation uncertainty was assumed to result mainly from differences in the evaluation procedures. The good agreement of the MACS data for ^{41}K obtained with the normalized cross sections from JEFF-3.3 and JENDL-4.0 justified an extrapolation uncertainty of $\pm 1\%$. The corresponding results for ^{45}Sc (columns 2 to 4 in Table VIII) exhibit deviations from the adopted average, particularly at high thermal energies, where the MACS values become sensitive to theoretical descriptions beyond the experimental TOF results. Based on the differences between the MACS data obtained with the evaluated cross sections, larger extrapolation uncertainties were considered for ^{45}Sc , reaching 3% at 50 keV and increasing to about 7% at 100 keV. Accordingly, the overall uncertainty starts to be dominated by the extrapolation above $kT = 50$ keV. The quoted uncertainties of the MACS values

 TABLE VII. MACS values of the $^{41}\text{K}(n,\gamma)^{42}\text{K}$ reaction^a (in mb) compared to the KADoNiS compilation [7].

Thermal energy (keV)	This work	KADoNiS ^b [7]
5	98.4 ± 2.8	92.8
10	54.7 ± 1.6	52.0
15	38.1 ± 1.1	37.6
20	28.8 ± 0.8	30.4
25	23.0 ± 0.7	26.0
30	19.2 ± 0.6	23.2 ± 0.8
40	16.6 ± 0.5	19.7
50	12.6 ± 0.4	17.6
60	11.2 ± 0.4	16.1
80	9.8 ± 0.3	14.2
100	9.1 ± 0.3	12.8

^aCalculated with the normalized (n,γ) cross section of JEFF-3.3 (identical to results obtained with JENDL-4.0).

^bRenormalized to present gold reference cross section.

in Tables VII and VIII are composed of the uncertainties of the measurement and of the extrapolation.

VI. THE ROLE OF LIGHT ELEMENTS IN THE s PROCESS

The influence of the light elements as potential neutron poisons for the s process have been studied for AGB as well as for massive stars. Based on a general discussion of this effect, the influence of the present MACS values is detailed for both s -process scenarios.

A. AGB stars

The abundance distribution of the main s component produced by AGB stars has been calculated with an updated post-processing code described in Ref. [38]. In this approach, the s abundances are obtained by averaging the results from stellar models for stars with initial masses $M = 1.5M_{\odot}$ and $3M_{\odot}$ and a metallicity $[\text{Fe}/\text{H}] = -0.3$. To characterize the s -process conditions between thermal instabilities, which contributes about 95% of the overall neutron exposure, the specific choice for the ^{13}C pocket has been adopted from [38] as well. This approach has been shown to provide a good approximation of the main s component in the solar system, and can be used to investigate the effect of individual MACS values by comparison with the abundances obtained with an initial or “standard” set of cross sections.

Within this AGB scenario, the potential neutron absorption by each of the light isotopes between ^{12}C and ^{56}Fe was determined one by one by setting the respective cross section to zero. As summarized in Table IX there are only a few reactions, which contribute notably to the poisoning effect in AGB stars, i.e., the (n,p) cross section of ^{14}N and the (n,γ) cross sections of ^{22}Ne , ^{23}Na , and ^{55}Mn . The strongest poisons are found to be ^{14}N and ^{22}Ne , the first due to its large (n,p) cross section and the latter due to its comparably high abundance.

The revised (n,γ) cross sections of ^{41}K and ^{45}Sc are affecting the respective s abundances by -2% and $+15\%$, respectively. But because the s process in AGB stars contributes only a few percent of solar K and Sc, the overall effect on the neutron balance of the s process is marginal in both cases.

In Fig. 4, the effect of the dominant poisons are illustrated by the abundance variations of selected s -only isotopes between Sr and Pb. If a strong neutron poison is eliminated, more neutrons are available for the s process. The higher s efficiency translates into a reduction of the s contribution to $^{86,87}\text{Sr}$ and consequently to an enhancement of the ^{208}Pb abundance, but affects the bulk of the s abundances only marginally.

At lower metallicities, the impact of neutron poisons becomes more important because of the higher relative abundances of the primary isotopes produced during stellar burning itself. This adds ^{12}C , $^{24,25}\text{Mg}$, and especially ^{16}O to the list of strong poisons. For a metallicity $[\text{Fe}/\text{H}] = -2.3$, these isotopes are largely affecting the whole s distribution as shown in Table IX. Significant abundance changes are also caused by ^{17}O , ^{33}S , ^{37}Ar via (n,α) , by ^{19}F via (n,γ) , and by ^{36}Cl via (n,p) .

TABLE VIII. MACS values of the $^{45}\text{Sc}(n,\gamma)^{45}\text{Sc}$ reaction (in mb) obtained with the normalized neutron capture cross sections of various databases compared to the KADoNiS compilation [7].

Thermal energy (keV)	JEFF-3.3	ENDF/B-7.1	JENDL-3.3	This work ^a	KADoNiS ^b [7]
5	176	174	176	175 ± 5	240
10	124	124	124	124 ± 4	162
15	96.7	95.8	96.7	96.4 ± 2.8	122
20	80.5	79.2	80.6	80.1 ± 2.3	100
25	69.3	68.2	69.8	69.1 ± 2.0	84
30	61.3	60.5	62.0	61.3 ± 1.8	73 ± 5
40	50.0	50.6	51.4	50.7 ± 1.5	57
50	42.6	44.3	44.4	43.8 ± 1.7	46
60	37.1	39.7	39.5	38.8 ± 2.2	40
80	29.9	33.0	32.7	31.9 ± 2.2	33
100	25.2	28.0	28.3	27.2 ± 2.1	28

^aAverage of columns 2 to 4.^bRenormalized to present gold reference cross section.

B. Massive stars

Massive stars ($M > 10M_{\odot}$) are known to produce most of the s -process abundances between Fe and Sr, the so-called weak s -process component (see [3] and references therein). Neutrons are produced in $^{22}\text{Ne}(\alpha, n)^{25}\text{Mg}$ reactions, first in the late phases of convective core-He burning, and subsequently during convective shell-C burning. The most abundant isotopes are ^{16}O , ^{12}C , $^{20,22}\text{Ne}$, $^{25,26}\text{Mg}$ and ^{16}O , ^{20}Ne , ^{23}Na , ^{24}Mg at the end of core-He and shell-C burning, respectively.

The impact of the present results on the weak s process in massive stars was investigated by means of a $25M_{\odot}$ model with an initial metal content $[\text{Fe}/\text{H}] = -2$ [40]. It turned out that the poisoning effects on the s abundances above the Fe seed are also marginal. The only significant changes in the s abundances are found in the vicinity of the investigated isotopes. The abundances calculated with the previous MACS

data and after implementation of the new results differ by up to 20%.

The largest abundance change due to the revised MACS values is about 20% for ^{41}K , whereas only a minor change is found for ^{45}Sc . The respective error bars in Fig. 5 correspond to the effect of a 1σ variation of the new MACS. Propagation effects of up to 5% are obtained for the isotopes of Ca with uncertainties of less than 1%.

VII. SUMMARY

The activation method has been used to measure the (n,γ) cross sections of ^{41}K and ^{45}Sc in a quasistellar neutron spectrum corresponding to a thermal energy of $kT = 25$ keV with significantly improved accuracy compared to previous data. These results have been used to normalize the evaluated energy-dependent cross sections from the data libraries ENDF,

TABLE IX. The effect of main neutron poisons^a in AGB stars illustrated by the abundances of selected s -only isotopes (in %).

Isotope	ST ^b	^{14}N	^{22}Ne	^{23}Na	^{55}Mn	^{12}C	^{16}O	^{24}Mg	^{25}Mg
Metallicity $[\text{Fe}/\text{H}] = -0.3$									
^{86}Sr	59	55	50	55	53	59	60	57	57
^{87}Sr	59	55	50	55	53	59	59	57	57
^{96}Mo	99	97	96	97	97	99	97	99	99
^{134}Ba	108	109	111	110	113	109	114	107	108
^{136}Ba	109	110	114	111	114	109	110	109	109
^{204}Pb	88	93	92	90	91	88	89	89	89
^{208}Pb	47	58	55	51	53	48	48	49	49
Metallicity $[\text{Fe}/\text{H}] = -2.3$									
^{86}Sr	6	4	120	33	15	3	3	20	13
^{87}Sr	4	3	90	22	10	2	2	14	9
^{96}Mo	17	21	190	33	7	18	17	26	21
^{134}Ba	18	24	141	26	7	22	27	23	21
^{136}Ba	22	28	158	30	9	25	30	27	25
^{204}Pb	133	123	182	113	165	129	127	118	126
$^{208}\text{Pb}^c$	7002	6536	10884	15384	16662	6815	6774	11709	10090

^aCalculated by setting MACS of poisoning isotope in line 1 to zero.^bStandard case obtained with full set of MACS values. All values normalized to a ^{150}Sm abundance of 100%.^cNote that about half of solar ^{208}Pb is produced by low-mass, low-metallicity AGB stars [1,39].

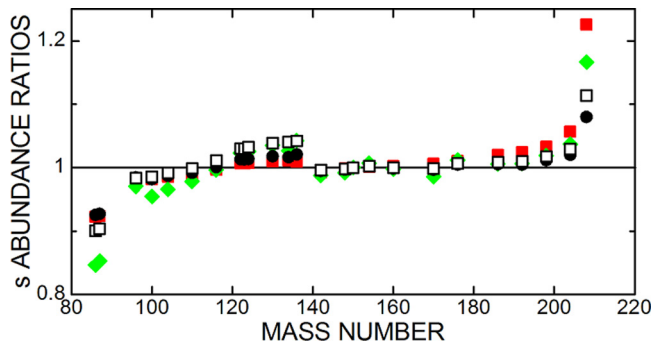


FIG. 4. The effect of the main neutron poisons ^{14}N (full squares), ^{22}Ne (diamonds), ^{23}Na (circles), and ^{55}Mn (open squares) in AGB stars with half of the solar metallicity $[\text{Fe}/\text{H}] = -0.3$. Plotted are the abundance variations of the s -only isotopes after the neutron cross sections of a particular poison was set to zero.

JEFF, and JENDL. Maxwellian averaged cross sections were then calculated over a range of thermal energies from $kT = 5$ to 100 keV. Compared to the 30 keV values in the KADoNiS database, the new MACS results are 15% and 13% smaller for ^{41}K and ^{45}Sc , respectively. In general, this seems to support a systematic trend that older TOF measurements have underestimated the background due to scattered neutrons. As this problem is characteristic of the resonance-dominated cross sections of light and intermediate-mass nuclei (see, e.g., [35–37]), it can give rise to a significant cumulative effect on the s -process neutron balance. Accordingly, the determination of accurate (n, γ) cross sections in the mass region $A < 56$ remains a continuing challenge. This holds particularly for the yet unmeasured cross sections of ^{38}Ar and ^{40}K as well as generally for isotopes with cross section uncertainties of more than 10%.

The role of the light isotopes between ^{12}C and ^{56}Fe , which represent potential neutron poisons for the s process, have been investigated with stellar models for thermally pulsing AGB stars as well as for massive stars. In both scenarios, the most important poisons are found among the abundant C, O, Ne, Na, and Mg isotopes, whereas the impact of the present results remains marginal.

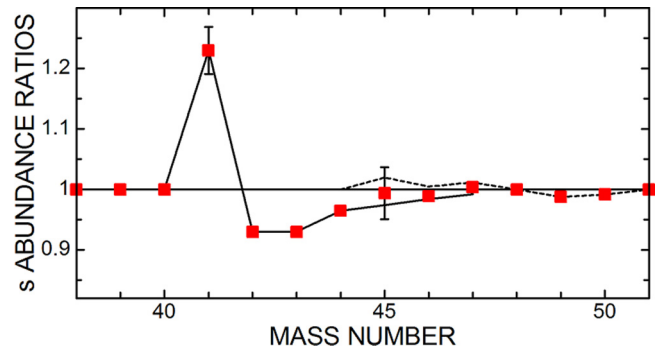


FIG. 5. The s -abundance ratios in a $25M_{\odot}$ star obtained with the previous set of MACS data and after implementation of the new results (solid squares). The individual response of ^{41}K and ^{45}Sc is indicated by the solid and dashed lines, respectively.

ACKNOWLEDGMENTS

We thank D. Roller, E.-P. Knaetsch, and W. Seith for their support during the measurements. S.B. acknowledges financial support from JINA (Joint Institute for Nuclear Astrophysics, University of Notre Dame, IN) and KIT (Karlsruhe Institute of Technology, Karlsruhe, Germany). M.P. acknowledges support from NuGrid by NSF Grant No. PHY 09-22648 (Joint Institute for Nuclear Astrophysics, JINA), NSF Grant No. PHY-1430152 (JINA Center for the Evolution of the Elements), and EU MIRG-CT-2006-046520. He also appreciates support from the “Lendület-2014” Programme of the Hungarian Academy of Sciences (Hungary) and from SNF (Switzerland). M.P. also acknowledges PRACE, through its Distributed Extreme Computing Initiative, for resource allocations on Sisu (CSC, Finland), Archer (EPCC, UK), and Beskow (KTH, Sweden). M.P. acknowledges the support of STFC’s DiRAC High Performance Computing Facilities; DiRAC is part of the National E-infrastructure. Ongoing resource allocations on the University of Hull’s High Performance Computing Facility—viper—are gratefully acknowledged.

- [1] R. Gallino *et al.*, *Astrophys. J.* **497**, 388 (1998).
- [2] A. I. Karakas and J. C. Lattanzio, *Pub. Astron. Soc. Aust.* **31**, e030 (2014).
- [3] F. Käppeler, R. Gallino, S. Bisterzo, and W. Aoki, *Rev. Mod. Phys.* **83**, 157 (2011).
- [4] C. Arlandini *et al.*, *Astrophys. J.* **525**, 886 (1999).
- [5] E. Zinner, *Annu. Rev. Earth Planet. Sci.* **26**, 147 (1998).
- [6] E. Zinner, in *Treatise on Geochemistry, Vol. 1*, 2nd ed., edited by H. Holland and K. Turekian (Elsevier, New York, 2014), p. 181.
- [7] I. Dillmann, R. Plag, F. Käppeler, and T. Rauscher, in *EFNUDAT Fast Neutrons – Scientific Workshop on Neutron Measurements, Theory & Applications*, edited by F.-J. Hamsch (JRC-IRMM, Geel, 2009), pp. 55–58, <http://www.kadonis.org>
- [8] R. Reifarh, M. Heil, C. Forssen, U. Besserer, A. Couture, S. Dababneh, L. Dorr, J. Gorres, R. C. Haight, F. Kappeler, A. Mengoni, S. O’Brien, N. Patronis, R. Plag, R. S. Rundberg, M. Wiescher, and J. B. Wilhelmy, *Phys. Rev. C* **77**, 015804 (2008).
- [9] E. Uberseder, M. Heil, F. Kappeler, J. Gorres, and M. Wiescher, *Phys. Rev. C* **75**, 035801 (2007).
- [10] M. Heil, R. Plag, E. Uberseder, R. Gallino, S. Bisterzo, A. Juseviciute, F. Kappeler, C. Lederer, A. Mengoni, and M. Pignatari, *Phys. Rev. C* **90**, 045804 (2014).
- [11] M. Heil *et al.*, *Pub. Astron. Soc. Aust.* **26**, 243 (2009).
- [12] D. Stuepegia, M. Schmidt, C. Keedy, and A. Madson, *J. Nucl. Energy* **22**, 267 (1968).
- [13] R. Macklin, N. Lazar, and W. Lyon, *Phys. Rev.* **107**, 504 (1957).

- [14] R. Booth, W. Ball, and M. Mac Gregor, *Phys. Rev.* **112**, 226 (1958).
- [15] A. Chaubey and M. Sehgal, *Phys. Rev.* **152**, 1055 (1966).
- [16] OECD Nuclear Energy Agency, Paris, <https://www.oecd-neo.org/dbdata/jeff/>
- [17] N. Iwamoto, JAERI-Report, <https://www.ndc.jaea.go.jp/jendl/j40/j40.html>
- [18] R. Macklin, *Nucl. Sci. Eng.* **88**, 129 (1984).
- [19] J. Perkin, *J. Nucl. Energy* **17**, 349 (1963).
- [20] S. Romanov and F. Shapiro, *Sov. J. Nucl. Phys.* **1**, 159 (1965).
- [21] M. Kenny, B. Allen, and R. Macklin, *Aust. J. Phys.* **30**, 605 (1977).
- [22] M. Chadwick *et al.*, *Nucl. Data Sheets* **112**, 2887 (2011).
- [23] H. Beer and F. Käppeler, *Phys. Rev. C* **21**, 534 (1980).
- [24] W. Ratynski and F. Käppeler, *Phys. Rev. C* **37**, 595 (1988).
- [25] I. Dillmann *et al.*, *Nucl. Data Sheets* **120**, 171 (2014).
- [26] C. Massimi *et al.*, *Eur. Phys. J. A* **50**, 124 (2014).
- [27] C. Massimi, C. Domingo Pardo, M. Calviani, and the n_TOF collaboration, *Phys. Rev. C* **81**, 044616 (2010).
- [28] C. Lederer *et al.*, *Phys. Rev. C* **83**, 034608 (2011).
- [29] P. Jiménez-Bonilla and J. Praena, in *Nuclei in the Cosmos XIII*, edited by Zs. Fülöp (SISSA, Trieste, 2015), PoS(NIC XIII)102.
- [30] B. Singh and J. Cameron, *Nucl. Data Sheets* **92**, 1 (2001).
- [31] S.-C. Wu, *Nucl. Data Sheets* **91**, 1 (2000).
- [32] Z. Chunmei, *Nucl. Data Sheets* **95**, 59 (2002).
- [33] W. Dixon, *Nucleonics* **8**, 68 (1951).
- [34] NIST, <http://www.nist.gov/pml/data/xraycoef/index.cfm>
- [35] P. E. Koehler, R. R. Winters, K. H. Guber, T. Rauscher, J. A. Harvey, S. Raman, R. R. Spencer, J. C. Blackmon, D. C. Larson, D. W. Bardayan, and T. A. Lewis, *Phys. Rev. C* **62**, 055803 (2000).
- [36] K. Guber *et al.*, *Nucl. Instrum. Methods B* **241**, 218 (2005).
- [37] K. Guber *et al.*, in *Nuclear Data for Science and Technology*, edited by R. Haight *et al.*, AIP Conf. Ser. No. 769 (AIP, New York, 2005), p. 1706.
- [38] S. Bisterzo *et al.*, *Mon. Not. R. Astron. Soc.* **449**, 506 (2015).
- [39] C. Travaglio *et al.*, *Astrophys. J.* **549**, 346 (2001).
- [40] M. Pignatari *et al.*, *Astrophys. J.* **762**, 31 (2013).